Radiative Cooling of a Hydrogen Plasma in a Shock Tube

George H. Stickford Jr.*
Battelle Columbus Laboratories, Columbus, Ohio

A method of computing radiative cooling of a hydrogen plasma, assuming quasi-isothermal radiative transfer, is described. In this approach, the flux divergence is evaluated using the isothermal solution to the equation of radiative transfer. With this simplification, coupled with the exponential approximation, nongray radiative cooling calculations in geometrically complex flowfields can be easily made. A comparison with nonisothermal calculations for a plane parallel slab indicates good agreement for temperature gradients up to 300 K/cm. Further comparisons with shock-tube data obtained in the Jet Propulsion Laboratory (JPL) high-performance shock-tube facility are presented.

Nomenclature

A_1, A_2 = constants derived from exponential approximation
$b_{1/2}$ = half-width of spectral line profile
B = Planck or blackbody function, Eq. (7)
c = speed of light, 2.998×10^{10} cm/sec
d = diameter of cylindrical test slug
div$q$ = flux divergence, Eq. (5)
h = Planck's constant, 6.625×10^{-27} erg-sec
h = gas enthalpy
I_λ = specific radiative intensity, erg/sec/μm/st/cm^2, Eq. (4)
k = Boltzman's constant, 1.38×10^{-16} ergs/deg
K_λ = effective absorption coefficient, including induced emission. Eq. (4)
ℓ = length of cylindrical test slug
L = radiation path length
Ne = electron number density, 1/cm^3
N_j^i = number density of species j, energy state i
P = pressure
q = integrated flux divergence
R = gas constant, Eq (16); radial coordinate variable
t = laboratory time from arrival of shock wave
T = gas temperature
u = gas velocity in x direction
V_s = shock velocity
x = axial coordinate
Δx = finite element thickness
r, θ, φ = polar coordinates
λ = wavelength
ξ = test slug length-to-diameter ratio, ℓ/d
$\sigma_j^i(\lambda)$ = optical cross section of species j, energy state i, at wavelength λ, cm^2
χ = nondimensional axial position, x/ℓ
Ω = solid angle

Superscripts

i = properties of the ith element
$1, n$ = the boundary elements

Introduction

THE increased interest in outer-planet exploration has provided an impetus to the development of high-performance shock-tube facilities. It was this impetus which led to the development of the conical-arc shock-tube driver by Menard[1] in 1970; this was the first shock-tube facility to produce shock speeds in excess of 20 km/sec with a usable test slug. Useful data were obtained[2] at shock speeds up to 35 km/sec in a test gas composed of a hydrogen-helium mixture. A subsequent development by Liebowitz,[3] using an annular arc driver, led to an equally significant increase in shock-tube performance. Shock speeds of 50 km/sec have been obtained in the 15.2-cm-diam Jet Propulsion Laboratory (JPL) shock tube at an initial pressure of 1.0 mm Hg.

The availability of shock-tube facilities capable of duplicating Jovian entry speeds makes it possible to perform many interesting and necessary experiments associated with the complex fluid dynamics and chemical kinetics of an entry vehicle shock-layer flow. A recent study[2] has explored the nonequilibrium flow behind the normal shock wave over a range of pressures and shock velocities and has demonstrated that, under certain conditions, the nonequilibrium relaxation time is much larger than expected. Nonequilibrium effects would therefore be more important with regard to outer-planet entry heating than previously expected.

A second area of uncertainty exists with regard to radiative cooling of the shock-layer flowfield. Radiative cooling of the gas in the bow shock region of a Jovian entry probe will, to some degree, reduce the total heating experienced by the probe. Accurate predictions of this phenomenon are very difficult because of the coupling of the radiative transfer equation with the flow equations. Several simplifying assumptions generally are needed to obtain a solution to the resulting set of integro-differential equations. Experimental verification of such solution will be required before they can be applied with confidence. The shock tube, with its ability to duplicate Jovian entry conditions, can provide data with which to compare calculations.

This paper describes a calculation technique developed to solve the coupled fluid-dynamic-radiative transfer equations. The method has been applied to the prediction of radiative cooling in a hypervelocity shock-tube test slug composed of a hydrogen-helium gas mixture, at plasma conditions approaching those expected to occur in a Jovian entry probe shock layer.

Shock-Tube Flow Model

Energy Equation

Radiative cooling influences the conservation equations of a fluid-dynamic system through the energy equation, given for steady flow as

$$\rho u [\, dh/dx + u\,(du/dx)\,] + \text{div}\, q = 0 \qquad (1)$$

Presented as Paper 75-40 at the AIAA 13th Aerospace Sciences Meeting, Pasadena, Calif. January 20-22, 1975; submitted February 5, 1975; revision received June 4, 1975. This work was supported by the California Institute of Technology, Jet Propulsion Laboratory, Pasadena, Calif.

Index categories: Radiative Coupled Flows and Heat Transfer; Radiation and Radiative Heat Transfer.

*Staff Scientist, Fluid and Thermal Sciences Section.

where div$q$ is the flux divergence term, or the loss of energy due to radiative transfer. Here the flow variables are treated as one-dimensional, whereas div$q$ is necessarily three-dimensional. The radiative loss term is expressed as[4]

$$\text{div}q = -\int_\Omega \int_\lambda \frac{\partial I_\lambda}{\partial R}\, d\lambda d\Omega \tag{2}$$

and $\partial I_\lambda/\partial R$ is given by the equation of radiative transfer:

$$\partial I_\lambda/\partial R = K_\lambda (I_\lambda - B_\lambda) \tag{3}$$

The effective absorption coefficient, given by K_λ, is corrected to include induced emission.

The addition of the flux divergence term to the conservation equations changes the nature of the equations in that the original set of differential equations becomes a set of integro-differential equations which are extremely difficult and time-consuming to solve, even with modern high-speed computers. Thus, it is appropriate to examine certain simplifying assumptions which lead to practical solutions of this problem.

Most of the methods used to evaluate the flux-divergence term utilize the assumption that the gas absorption coefficient is constant (gray gas) or at least constant over specific wavelength bands (the multistep or multiband absorption coefficient models). The accuracy of these assumptions is questionable because of the seemingly random nature of the location of discrete line radiation and the fact that the absorption coefficient can vary several orders of magnitude over very small wavelength intervals. Of course, the band models can be made to produce relatively accurate integrated radiative emission at specific temperature, density, and optical path length conditions by proper choice of band constants. Nevertheless, a simple model cannot be expected to produce accurate results over all conditions needed for the radiative cooling calculation. For example, the largest energy losses through radiation from an entry vehicle shock layer or shock-tube test slug occur at the flow boundaries. Thus, the most important path lengths which must be considered are near zero. Most models, however, are developed to reproduce radiative intensity results at the long path lengths and may not be accurate at shorter path lengths.

If one intends to use the full spectral details of the gas absorption coefficient, most of the common methods of evaluating the flux divergence become unmanagable, or, at best, very time-consuming. As an example, the differential approximation replaces the flux divergence integral with a series, thus reducing the integro-differential energy equation to a pure differential. The method typically is used along with the gray-gas assumption, but has been applied to a shock-tube flow by Chien and Compton[5] for a four-band spectral model in air. The differential approximation is shown to agree quite well with "exact" calculations; however, in both cases the four-band absorption coefficient model is used. Although the differential approximation can reduce the computer time by a factor of 10 compared to the "exact" calculations, the necessary computational time is still prohibitive (several hours on an IBM 7094) if one considers a several-hundred-point spectrum.

Evaluation of Flux Divergence Term

The difficulty of the flux divergence integral is that the intensity must be evaluated in every direction at each point, and every calculation must be repeated at each wavelength. However, if one assumes that the radiative transfer within the flowfield can be described adequately by isothermal transfer, the flux divergence term can be simplified tremendously.

Assuming isothermal radiative transfer at each point within the flowfield, Eq. (3) can be solved to give the intensity as

$$I_\lambda = B_\lambda (1 - e^{-K_\lambda r}) \tag{4}$$

The flux divergence thus becomes

$$\text{div}q = \int_\lambda K_\lambda B_\lambda \left(\int_\Omega e^{-k_\lambda r} d\Omega \right) d\lambda \tag{5}$$

It is necessary in the present study to evaluate the flux divergence along the centerline of the shock-tube test slug. The geometry of the test slug is indicated in Fig. 1, where ℓ is the test slug length, and d is the tube diameter. The shock is located at $x=0$, flow is in the $+x$ direction, and the contact surface (end of test slug) is located at $x=\ell$. The test slug boundaries are assumed to transmit or absort all incident radiation. Using an exponential approximation for a cylindrical geometry, the interior integral in Eq. (5) can be replaced with a simple sum of exponential terms, and the flux divergence term becomes

$$\text{div}q = 2\pi \int_\lambda K_\lambda B_\lambda (e^{-A_1 K_\lambda d} + e^{-A_2 K_\lambda d})\, d\lambda \tag{6}$$

The exponential approximation is simply a mathematical approximation where the integral of an exponential function is replaced by a sum of exponential functions. This type of approximation is common in radiative transfer problems and is described in detail in Ref. 4.

The present application is somewhat unique, in that the integral is evaluated over a specific volume, that is, the cylindrical shock-tube test slug. The A's have been evaluated analytically by solving the following integral equation in the limit of $K_\lambda \ll 1$:

$$2\pi (e^{-A_1 K_\lambda d} + e^{-A_2 K_\lambda d})$$

$$= \int_0^{2\pi} \int_0^{\pi} e^{-K_\lambda r(\theta)} \sin\theta\, d\theta d\varphi$$

$$= 2\pi \left\{ \int_0^{\pi/2} e^{-K_\lambda r(\theta)} \sin\theta d\theta + \int_{\pi/2}^{\pi} e^{-K_\lambda r(\theta)} \sin\theta d\theta \right\}$$

where $d\Omega$ has been replaced by $\sin\theta d\theta\varphi$, and r, θ, φ are spherical coordinates as shown for the shock-tube test slug in Fig. 1 (φ is rotation about the x-axis). At every point x the integration must be performed over the entire volume of the test slug. With the quasi-isothermal assumption, K_λ does not vary with location and the integration depends only on the geometry. In principle, the integration can be carried out, once and for all, for any geometry, with K_λ and x as parameters. This is the key to the simplification offered by the quasi-isothermal approach.

For the cylindrical geometry of a shock-tube test slug, $r(\theta)$ can be expressed as

$$\frac{r(\theta)}{d} = \frac{\xi(1-\chi)}{\cos\theta}$$

$$\text{for } 0 \le \theta \le \cos^{-1}\left\{ \frac{2\xi(1-\chi)}{[4\xi^2(1-\chi)^2+1]^{1/2}} \right\}$$

$$\frac{r(\theta)}{d} = \frac{1}{2\sin\theta}$$

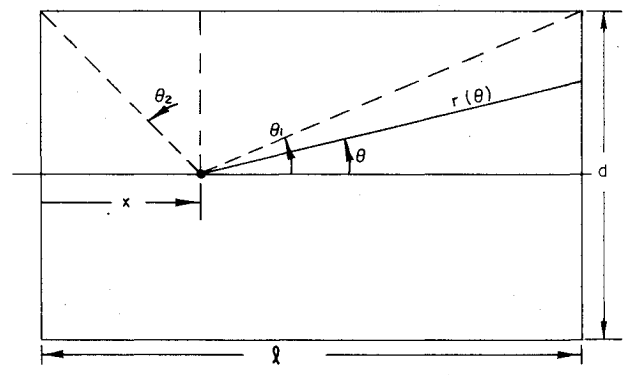

Fig. 1 Coordinate system for volume integration over shock-tube test slug.

$$\text{for } \cos^{-1}\left\{\frac{2\xi(1-\chi)}{[4\xi^2(1-\chi)^2+1]^{1/2}}\right\} \leq \theta \leq \frac{\pi}{2}$$

$$\frac{r(\theta)}{d} = \frac{1}{2\sin\theta} \text{ for } \frac{\pi}{2} \leq \theta \leq \cos^{-1}\left\{\frac{2\xi\chi}{[4\xi^2\chi^2+1]^{1/2}}\right\}$$

$$\frac{r(\theta)}{d} = \frac{\xi\chi}{-\cos\theta} \text{ for } \cos^{-1}\left\{\frac{2\xi\chi}{4\xi^2\chi^2+1]^{1/2}}\right\} \leq \theta \leq \pi$$

Replacing e^a with $1-a$, and integrating over the preceding boundaries, the following values of A_1 and A_2 are obtained:

$$A_1 = \xi(1-\chi)\left\{\ln\left[\frac{[4\xi^2(1-\chi)^2+1]^{1/2}}{2\xi(1-\chi)}\right]\right\} + \tfrac{1}{2}\tan^{-1}[2\xi(1-\chi)]$$

$$A_2 = \xi\chi\left\{\ln\left[\frac{[4\xi^2\chi^2+1]^{1/2}}{2\xi\chi}\right]\right\} + \tfrac{1}{2}\tan^{-1}(2\xi\chi)$$

Although these results were obtained for small K_λ, numerical calculations have demonstrated that they are accurate, to within a few percent, for all values of K_λ for cylindrical geometries of $\xi \simeq 1$.

With this simplification, the flux divergence term, and therefore the energy equation, becomes strictly a function of x. The effects of geometry are contained in the terms A_1 and A_2; the divergence depends on temperature through K_λ and B_λ. The isothermal assumption applies only to the solution of the radiative transfer equation. This approach therefore is referred to as the quasi-isothermal assumption.

The flux divergence term can be thought of as being composed of two terms: an emission term and an absorption term. The emission term is the energy lost due to radiation from point x, and the absorption term is the gain of energy at point x due to absorption of radiation originating from the other regions of the flowfield. The quasi-isothermal assumption affects only the absorption term, in that the radiation originating from other regions is calculated by assuming that these regions are at a temperature equal to the temperature at point x. If the temperature at x is below the average for the flowfield, the flux divergence will be overestimated. Likewise, if the temperature at x is above average, the flux divergence will be underestimated. Thus, this method has an inherent compensating characteristic when the calculation is carried over the entire flowfield. Furthermore, in the limit of optically thin or optically thick plasmas, this method becomes exact, since the absorption of radiation at point x originating from extended regions of the plasma becomes zero.

The evaluation of the quasi-isothermal flux divergence term requires only an integration over wavelength of terms containing B_λ and K_λ. The Planck function is given as

$$B_\lambda = (2hc^2/\lambda^5)(e^{(hc/\lambda kT)} - 1)^{-1} \quad (7)$$

The effective absorption coefficient can be expressed as

$$K_\lambda = (1 - e^{-hc/\lambda kT}) \sum_i \sum_j \sigma_j^i(\lambda) N_j^i \quad (8)$$

where σ_j^i is the absorption cross section of the i th energy level of the jth species, N_j^i is the number density of the ith energy level of the jth species, and the exponential term is the correction for induced emission. At each wavelength this summation must be evaluated over all of the energy levels of all species present in the plasma.

Since the current study was limited to hydrogen radiation (the radiation due to a small percentage of helium is negligible), this task is reduced to considering two species, H and H^+ (H^- is also negligible). For the hydrogen atom, H, a total of nine lines are considered. For the ion H^+, there are seven free-bound cross sections and a free-free cross section included. Thus, there are a total of 17 radiative processes considered in Eq. (8). Specific details of the calculation of the various cross sections are presented in previous reports.[6,7]

The spectral detail of the absorption coefficient is obtained by evaluating K_λ, using Eq. (8), at approximately 250 points across the spectrum from 0.05 to 3.0 μm. The points used are carefully chosen, depending on the plasma temperature and electron density, to include the necessary detail and produce accurate results when compared with results obtained in Ref. 7. For example, each of the nine lines is treated by choosing eleven points over the line profile from λ_0, the line center, to $\lambda_0 \pm 8b_{1/2}$, eight times the half-width from the line center. Up to 75 additional points are selectively chosen to describe unusual features of the absorption coefficient spectrum, such as very broad lines, and sudden changes in continuum level at the series limits. Finally, up to 100 points are chosen at uniform energy increments in those parts of the spectrum which are not described already.

A typical absorption coefficient spectrum is presented in Fig. 2. The hydrogen spectral details are seen to be represented very well. In Fig. 3, the resultant integrated intensity for path lengths of 1 and 10 cm is compared with the more precise calculations obtained using the technique described in Refs. 7 and 8. The comparison at various thermodynamic conditions and path lengths, ranging down to 1 cm, shows that the calculations with less spectral detail generally agree to within a few percent and are never more than 10% from the more detailed calculations.

Example of Results for Plane Parallel Slab

The overall accuracy of the quasi-isothermal approximation has been investigated by analyzing the plane parallel slab. Nonisothermal calculations of flux divergence and integrated flux divergence have been made for a plane parallel slab 10 cm thick with a linear temperature distribution. The method used to obtain the nonisothermal

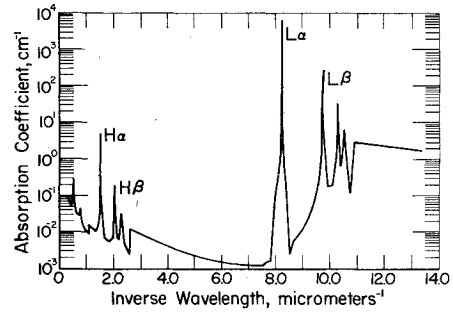

Fig. 2 Calculated absorption coefficient for Hydrogen, $T = 15{,}000$ K, $Ne = 0.248 \times 10^{18}$ l/cm^3.

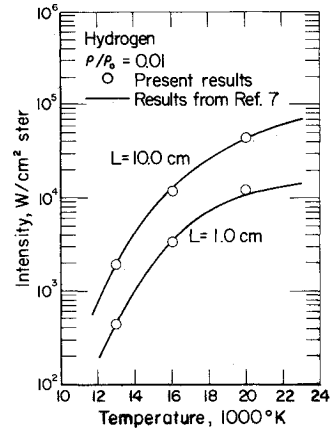

Fig. 3 Comparison of integrated intensity results with previous calculations.

results was to divide the slab into a number of finite elements over which the fluid properties are assumed constant. In this case, the radiative transfer equation, Eq. (3), has the solution (see Ref. 4, p. 476).

$$I_\lambda = I_\lambda(R)\exp\left(-\int_0^R K_\lambda \mathrm{d}r\right) + \int_0^R K_\lambda B_\lambda \exp\left(-\int_0^r K_\lambda \mathrm{d}r'\right)\,\mathrm{d}r \tag{9}$$

which, for finite elements with constant properties, becomes (in the positive direction)

$$I_\lambda^i = \sum_{\substack{j=1,\\ i-1}} \frac{K_\lambda^j B_\lambda^j \Delta x^j}{\cos\theta} \exp\left[-\sum_{k=j,i} \frac{K_\lambda^k \Delta x^k}{\cos\theta}\right] \tag{10}$$

The radiative intensity incident on the boundaries is zero. Again, the exponential approximation is utilized to remove the solid-angle integration in the flux divergence. In both the nonisothermal and quasi-isothermal cases, the integration of the exponential term is approximated by

$$\int_\Omega \exp(-K_\lambda d/\cos\theta)\,\mathrm{d}\Omega \doteq 4\pi\exp(-2K_\lambda d)$$

This approximation is about 12% high at $K_\lambda d = 0.1$ and about 12% low at $K_\lambda = 1.0$. At $K_\lambda d \ll 1.0$ the expression is exact. At $K_\lambda d \gg 1.0$ the approximation becomes very poor but is of no consequence, since the flux divergence goes to zero at this limit. Furthermore, it is noted that the approximation applies equally well to both the nonisothermal and quasi-isothermal calculations. Thus, the comparison of results for the two cases should be not influenced by this mathematical approximation.

For the nonisothermal case, the intensity at each point is obtained by evaluating Eq. (10) in either direction, for $\theta = 60°$; in the $+x$ direction

$$I_\lambda^i(+x) = 2\sum_{j=1,i} K_\lambda^j B_\lambda^j \Delta x^j \exp\left[-\sum_{k=j,i} 2K_\lambda^k \Delta x^k\right]$$

and in the $-x$ direction

$$I_\lambda^i(-x) = 2\sum_{j=i,n} K_\lambda^j B_\lambda^j \Delta x^j \exp\left[-\sum_{k=i,j} 2K_\lambda^k \Delta x^k\right]$$

A correction to these equations is required to account for reabsorption within the finite elements. This can be accomplished by setting

$$2K_\lambda^j B_\lambda^j \Delta x^j = B_\lambda^j[1 - \exp(-2K_\lambda^j \Delta x^j)]$$

in the first summation when

$$2K_\lambda^j \Delta x^j > 0.005.$$

The flux divergence is given by

$$\mathrm{div}\, q^i = 2\pi \int_\lambda K_\lambda [I_\lambda^i(+x) + I_\lambda^i(-x) - 2B_\lambda^i]\,\mathrm{d}\lambda \tag{11}$$

and the integrated flux divergence is simply

$$q^i = \sum_{j=1,i} \mathrm{div} q^j \Delta x^j \tag{12}$$

Calculations were made for a plane parallel slab geometry with a linear temperature distribution, constant pressure of approximately 2 atm, and a slab thickness of 10 cm. Since the flux divergence varies greatly at the boundaries and only slightly on the interior, the element size was varied linearly, such that the element on the boundary as 1/10 the width of the center element.

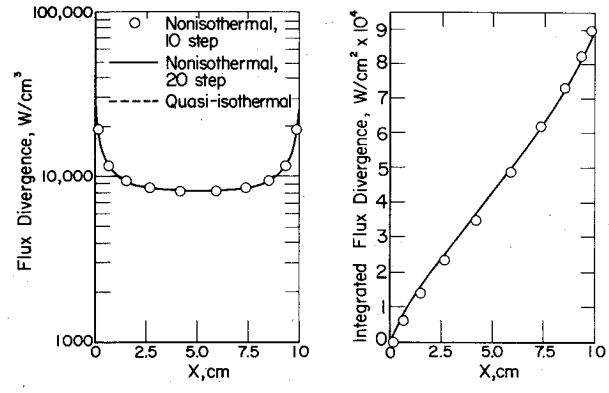

Fig. 4 Plane parallel slab flux divergence results for $T = 15{,}000$ K, $Ne = 0.248 \times 10^{18}$ 1/cm³, and $\Delta T/\Delta X = 0$.

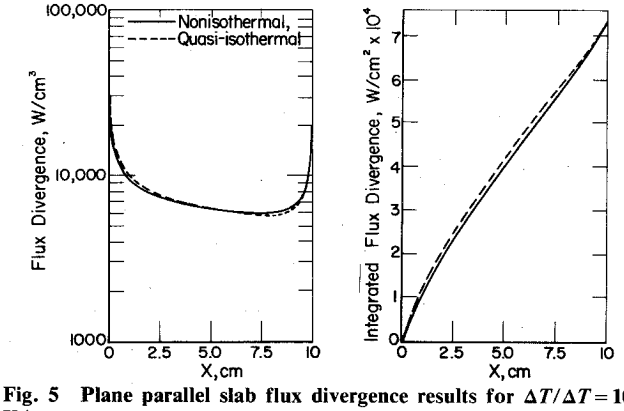

Fig. 5 Plane parallel slab flux divergence results for $\Delta T/\Delta T = 100$ K/cm.

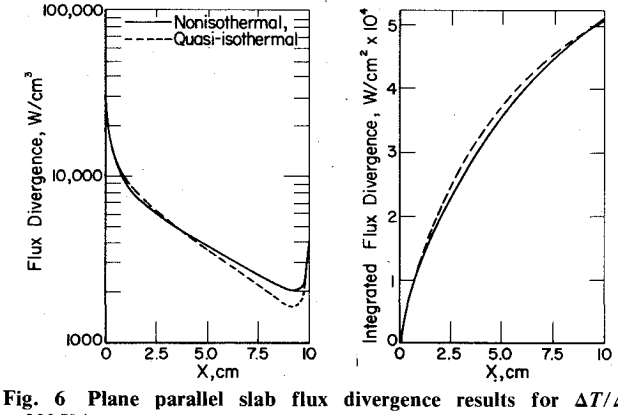

Fig. 6 Plane parallel slab flux divergence results for $\Delta T/\Delta X = 300$ K/cm.

As a check on the nonisothermal results, calculations were performed for a zero temperature variation through the slab. In this case, the quasi-isothermal calculation applies exactly and is used to gage the accuracy of the finite-element approach. The results are presented in Fig. 4 for a temperature of $T = 15{,}000$ K and $Ne = 0.248 \times 10^{18}$ cm^{-3}. The flux divergence and the integrated flux divergence (integrating left to right) are shown as a function of distance through the slab. The finite-element calculation was performed for both 10 and 20 elements. Using just 10 elements was found to result in errors of 3 to 4%, whereas the 20-element results were within 1/10% of the analytical quasi-isothermal results. In subsequent calculations, 20 elements were used to obtain the finite-element nonisothermal results.

Figures 5 and 6 present the results of calculations for a 100- and 300-K/cm linear drop in temperature from 15,000 K. The electron density was adjusted such that equilibrium prevailed.

The gas pressure was taken to be constant at 2 atm. The results show that for a 100-K/cm temperature variation the quasi-isothermal results for flux divergence are within 6% of the "exact" finite-element calculations. The integrated flux divergence in this case is off by only 3%. For the 300-K/cm case, the flux divergence deviates at one point by a maximum of 25%, whereas the integrated flux divergence differs by only 12%. It is noted that, for the most severe case (300 K/cm), the final value of integrated flux divergence for the quasi-isothermal results is within 3.5% of the nonisothermal result.

Description of Shock-Tube Results

Shock-Tube Flow Equations

The conservation equations for one-dimensional flow through a shock-tube test slug can be written as follows:

$$\rho u = \rho_2 u_2 \tag{13}$$

$$P = P_2 \tag{14}$$

$$h + (u^2/2) = h_2 + (u_2^2/2) - (q/\rho_2 u_2) \tag{15}$$

$$P/\rho = ZRT \tag{16}$$

where the subscript 2 refers to conditions immediately behind the shock, and q is the integrated flux divergence, obtained by integrating Eq. (6) from the shock to the point x. The momentum equation is simplified by assuming that the pressure is constant through the slug. This assumption was validated by computing the pressure drop for various conditions. The pressure variation was found to be approximately 1% of the initial pressure and, therefore, negligible.

The procedure for computing the test slug cooling is first to compute the equilibrium test slug conditions ("2" conditions) using the JPL thermochemistry program.[9] Next, the flux divergence distribution through the test slug was computed using the equilibrium conditions as the initial conditions. Using the conservation equations and the caloric and thermal equations of state, the new density and temperature distributions were computed. The new density and temperature then were used in the Saha equation to determine the new distribution of electron density. With these adjusted quantities, the flux divergence was recalculated and the foregoing procedure repeated. At the end of each iteration, the new temperature was compared with the previous value. The iteration was continued until the change in temperature was found to be below some prescribed value, usually 1% or less.

Facility and Instrumentation

The data to be presented were obtained in the JPL-arc-driven shock-tube facility. The arc driver used was developed by L. Liebowitz and is described in detail in Ref. 3. The driver, connected to the JPL 0.29 MJ capacitor bank, produced shock speeds in the range of 40 to 50 km/sec into 1.0 mm Hg initial pressure of hydrogen.

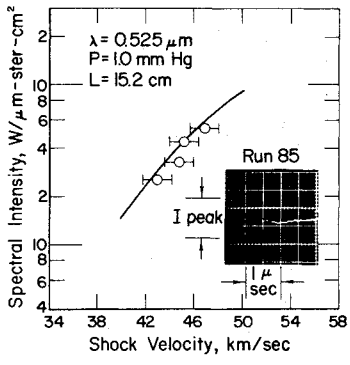

Fig. 7 Peak hydrogen continuum intensity measurements.

The shock tube consists of approximately 10 m of 15.2-cm i.d. stainless-steel tube. The initial pressure of hydrogen in the shock tube was measured with a precision oil manometer. Shock velocity was monitored at three points along the shock tube over a distance of approximatey 2 m. Because of the combination of several factors, the accuracy of the shock speed measurement was limited to uncertainties of ±5% percent. This uncertainty will be indicated in the data to be presented.

The continuum intensity measurements were made using an RCA 1P28 photomultiplier tube. The photomultiplier viewed the test slug through a window-and-slit configuration mounted on the side of the shock tube, viewing perpendicular to the axis of the shock tube. The size and spacing of the slits were chosen such that the spatial resolution of the region viewed by phototube was approximately 3 mm. The effective time resolution, based on a shock speed of 45 km/sec, was 67 nsec. The response time of the phototube and attendant circuitry was measured to be about 60 nsec.

The photomultiplier viewed the test slug through a narrow-band pass filter with peak transmission at 0.525 μm and a half-width of 50 Å. The total system was calibrated for absolute intensity using a Mole-Richardson carbon arc. Since the plasma intensity was 10 times brighter than the arc, it was necessary to place precision, neutral density filters in the view path during a run. These filters were calibrated by the manufacturer and guaranteed to be within a few percent of the stated transmission.

Discussion of Results

The spectral intensity measurements of hydrogen continuum intensity are presented in Fig. 7. The solid line is the calculated intensity, including the contribution of the hydrogen lines (H_α, H_β) and the negative ion at this wavelength. The symbols represent the peak value of intensity. The peak is reached shortly after the passage of the shock, followed by a decrease in intensity, presumably from radiative cooling. An example data trace is shown as an inset in Fig. 7.

Table 1 Run 58, $Vs = 45.2$ km/sec, slug length = 8 cm

t, sec	x, cm	Temp, K	h, ergs/g	Ne, l/cm^3	div$q$, W/cm^3
0.0	0.0	14,810	0.103×10^{14}	0.234×10^{18}	0.325×10^{6}
0.005	0.02	14,747	0.102	0.230	0.245×10^{5}
0.02	0.08	14,733	0.102	0.230	0.166
0.09	0.40	14,681	0.101	0.227	0.100
0.18	0.80	14,654	0.999×10^{13}	0.226	0.886×10^{4}
0.35	1.60	14,565	0.985	0.220	0.781
0.53	2.40	14,486	0.973	0.216	0.713
0.71	3.20	14,394	0.961	0.210	0.672
1.06	4.80	14,271	0.940	0.207	0.622
1.42	6.40	14,122	0.920	0.196	0.592
1.60	7.20	14,060	0.910	0.191	0.607

Table 2 Run 85, $Vs = 46.9$ km/sec, slug length = 6 cm

t, sec	x, cm	Temp., K	h, ergs/g	Ne, l/cm^3	div$q$, W/cm^3
0.0	0.0	15,220	0.110×10^{14}	0.268×10^{18}	0.390×10^{6}
0.004	0.02	15,164	0.110	0.264	0.345×10^{5}
0.01	0.06	15,149	0.110	0.264	0.238
0.06	0.30	15,100	0.109	0.261	0.141
0.13	0.60	15,057	0.108	0.258	0.121
0.25	1.20	15,000	0.106	0.256	0.108
0.36	1.80	14,926	0.105	0.251	0.995×10^{4}
0.51	2.40	14,857	0.104	0.247	0.934
0.77	3.60	14,726	0.102	0.244	0.875
1.02	4.80	14,588	0.999×10^{13}	0.232	0.827
1.15	5.40	14,529	0.989	0.228	0.863

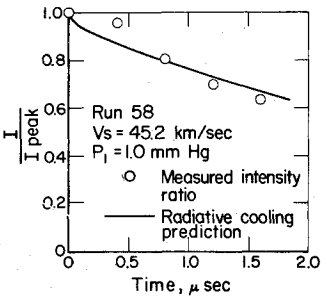

Fig. 8 Radiative cooling prediction compared with shock-tube data, run 58.

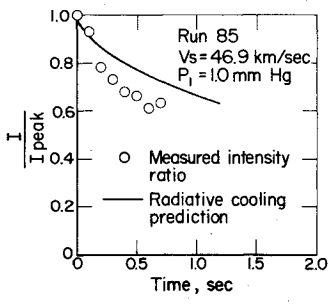

Fig. 9 Radiative cooling prediction compared with shock-tube data, run 85.

The peak intensity measurements agree fairly well with the equilibrium calculations; however, they fall consistently below the theory. This is not unexpected. Because of the combination of chemical nonequilibrium within the shock (projected to be approximately 50 nsec at these conditions,[2] and a finite system response time, coupled with the fact that the gas begins cooling before the peak intensity value is reached, one would expect the peak value to be somewhat below the equilibrium value.

It should be pointed out that the data in Fig. 7 represent only a fraction of the runs made during this test. On more than half the runs, the intensity profile was very erratic and did not correlate with the calculated equilibrium intensity. It was assumed that on these runs the contact surface turbulence prohibited the formation of a uniform test slug.

The decrease in continuum intensity from the peak value was examined for two of the four runs presented in Fig. 7. The intensity distributions of these two runs indicate a distinct test slug and were displayed on the oscilloscope trace with adequate time resolution to facilitate data reduction. For these two runs, the radiative cooling calculation was performed, and the results are given in Tables 1 and 2. The temperature variation through the test slug is seen to be only 100 K/cm for run 58 and 130 K/cm for run 85. Thus the quasi-isothermal approximation should be applicable for these data.

The continuum intensity variation was determined by assuming the intensity to be proportional to the square of the electron density, i.e.,

$$I_\lambda / I_\lambda \text{peak} = (\text{Ne}/\text{Ne}_{\text{equil}})^2$$

This relationship was found to accurately correlate hydrogen continuum intensity at the shock-tube contidions in this test. The resultant intensity distribution is shown in Figs. 8 and 9 as solid lines, along with the measured intensity ratio for the corresponding run. The results for run 58 (Fig. 8) agree fairly well with the measurements, whereas the results for run 85 tend to be slightly high. In either case, the calculations indicate that the maximum cooling rate occurs nearest the flow boundary (shock wave) as one would intuitively expect, whereas the data seem to indicate a maximum cooling rate at some later time. This may be due to the finite response time of the photomultiplier circuitry combined with the chemical nonequilibrium within the shock wave. These effects would tend to eliminate the cusp exhibited by the calculations at $t=0$ and produce a more rounded peak characteristic of the measurements.

The quasi-isothermal calculation has been demonstrated to accurately predict the radiative cooling for axial temperature variations of up to 300 K/cm in a plane parallel slab. However, the shock-tube test slug will experience a greater amount of cooling near the tube wall than along the centerline. As a result, a lateral temperature variation will develop. The sidewall intensity measurement in this case will be lower because of the presence of the cooler plasma near the boundaries.

Calculations by Chien and Compton,[5] for radiative cooling in a 5-cm shock tube with air as the test gas, indicate that the energy loss at the tube boundary can be as much as 30% more than the loss along the centerline. It is difficult to extrapolate their results to the conditions of the present experiment. Nevertheless, it is conceivable that the lateral temperature variation could cause the emitted intensity to be 10 to 20% low for the results of this experiment.

Conclusions

An approximate method of computing radiative cooling of a hydrogen plasma in a shock tube was described. The method differs from other approaches in that a detailed absorptoin coefficient model was used. The simplification is made by assuming that the equation of radiative transfer is adequately described by isothermal transfer, whereas the emission and absorption are evaluated at the local temperature, referred to as the quasi-isothermal assumption. The flux divergence term is simplified greatly by this assumption coupled with an exponential integral approximation.

Sample calculations for a plane parallel slab were compared with a nonisothermal, finite-element solution. The quasi-isothermal results agree surprisingly well with the nonisothermal calculations for temperature variations of up to 300 K/cm. The quasi-isothermal assumption should predict radiative cooling in shock-tube flows to accuracies of 10% or better when the temperature gradient is less than 300 k/cm. The applicability of this method to flows with larger temperature gradients is uncertain.

Calculations were compared with shock-tube data obtained in the JPL arc-driven shock tube. For one run, the data and calculations were in good agreement, whereas the calculations for the second run were approximately 20% high. A possible explanation for the discrepancy is the existence of a lateral temperature gradient across the diameter of the test slug because of greater cooling near the tube boundaries.

References

[1] Menard, W.A., "A Higher Performance Electric-Arc-Driven Shock Tube," *AIAA Journal, Vol. 9,* No. 10, Oct. 1971, p. 2096.

[2] Liebowitz, L.P., Menard, W.A., and Stickford, G.H., Jr., "Radiative Relaxation Behind Strong Shock Waves in Hydrogen-Helium Mixtures," *Ninth International Shock Tube Symposium,* Stanford University, *Research Developments in Shock Tube Research,* D. Bershader and W. Griffith, Stanford University Press, Stanford, Calif., 1973.

[3] Liebowitz, L.P., "Jupiter Entry Simulation with an ANAA Shock Tube," AIAA Paper 74-610, 1974.

[4] Vincenti, W.G. and Kruger, C.H., Jr., *Introduction to Physical Gas Dynamics,* Wiley, New York, 1965.

[5] Chien, K.Y. and Compton, D.L., "Flow in a Cylindrical Shock Tube with Radiative Energy Loss," *Proceedings of the 1970 Heat Transfer and Fluid Mechanics Institute,* 1970, Monterey, Calif., p. 278.

[6] Stickford, G.H., Jr. and Menard, W.A., "Bow Shock Composition and Rediative Intensity Calculations for a Ballistic Entry into the Jovian Atmosphere," AIAA Paper 68-787, 1968, Los Angeles, Calif.

[7] Stickford, G.H., Jr., "Total Radiative Intensity Calculations for 100% H_2 and 87% H_2—13% He," *Journal of Quantitative Spectroscopy and Radiative Transfer,* Vol. 12, 1972, p. 525.

[8] Stickford, G.H., Jr., "Total Radiative Intensity Calculations for 100% CO_2 and 90% CO_2-10 % N_2 *Journal of Quantitative Spectroscopy and Radiative Transfer,* Vol. 10, 1970, p. 249.

[9] Horton, T.W., "The JPL Thermochemistry and Normal Shock Computer Program," TR 32-660, 1964, Jet Propulsion Laboratory, Pasadena. Calif.